CHEMISTRY
A European Journal

A Journal of
ChemPubSoc Europe

Accepted Article

Title: Hydrogen-Bonding as Supramolecular tool for Robust OFET Devices

Authors: Soumyaditya Mula, Tianyan Han, Thomas Heiser, Patrick Lévêque, Nicolas Leclerc, A. P. Srivastava, Amparo Ruiz-Carretero, and Gilles Ulrich

To be cited as: *Chem. Eur. J.* 10.1002/chem.201900689

Link to VoR: http://dx.doi.org/10.1002/chem.201900689

Supported by
ACES

WILEY-VCH

10.1002/chem.201900689

WILEY-VCH

FULL PAPER

Hydrogen-Bonding as Supramolecular tool for Robust OFET Devices

Soumyaditya Mula,*[a][b][c] Tianyan Han,[d] Thomas Heiser,[d] Patrick Lévêque,[d] Nicolas Leclerc,*[a] A. P. Srivastava,[e] Amparo Ruiz-Carretero,[f] Gilles Ulrich*[a]

Abstract: In the present study, we demonstrated the effect of H-bonding in the semiconducting behaviour of a small molecule used in organic field-effect transistors (OFETs). For this study, a highly soluble dumbbell-shaped molecule, ***t*-Boc-TATDPP** based on *t*-Boc protected thiophene-DPP and triazatruxene (TAT) moieties was used. Two *t*-Boc groups of the molecule were removed by annealing at 200 °C which created a strong H-bonded network of **NH-TATDPP** supported by additional π-π stacking. These were characterised by TGA, UV-vis, IR, XRD and HR-TEM measurements. FETs were fabricated with a semiconducting channel made of ***t*-Boc-TATDPP** and **NH-TATDPP** separately. It is worth mentioning that the ***t*-Boc-TATDPP** film can be cast from solution and then it was annealed to get the other systems with **NH-TATDPP**, which makes easy to process the films with vacuum evaporation. More importantly, **NH-TATDPP** showed significantly higher hole mobilities compared to ***t*-Boc-TATDPP**. Interestingly, the high hole mobility in the case of **NH-TATDPP** was unaffected upon blending with $PC_{71}BM$. Thus, this robust hydrogen-bonded supramolecular network is likely to be useful in designing efficient and stable organic optoelectronic devices.

Introduction

It is well known that the hydrogen-bonding (H-bonding) is a highly specific tool for supramolecular organization of organic materials, the most common examples being biomolecules such as proteins and DNA. The effect of H-bonding mediated self-organization in the field of synthetic materials science are well studied,[1] however, this concept is relatively new in organic electronics field.[2] H-bonding interactions are very useful to enforce planarity of the molecules and to enhance the intermolecular interactions between them. This effectively helps in increasing the conjugation lengths and enforcing the molecular orientation as well as the packing of organic molecules, which enhances the device performance.[3] This also increases the morphology robustness, which is very important for the blend morphology stability as well as the stability of the performances of the device, a key factor for the commercialization of organic transistors and related devices like organic solar cells (OSCs). The objective of the present study is to demonstrate the effect of the H-bonding in the semiconducting behaviour of a small molecule used in organic field-effect transistors (OFETs).

DPP (**d**iketo**p**yrrolo**p**yrrole), a well-known high-performance organic pigment was developed in the 1980s.[4] Till now DPP-based molecules as well as polymers are one of the well-studied dyes as electronic materials for OFETs[3c, 5] and organic photovoltaics (OPVs)[4, 6] due to their superior charge transport properties and chemical stability. DPP is a small organic molecule with a planar π-electron core having two free amide groups in the opposite site of the molecules which make strong intermolecular interactions via N–H···O=C H-bonding. As a result it becomes insoluble in polar and non-polar solvents. This restricts their uses in solution processed applications. However, alkylation of the N-H group increases strongly their solubility. Another strategy to make them solution-processable consists in protecting their N-H function with a further cleavable group, such as *t*-Boc. Indeed, *t*-Boc group can be eliminated by heating (~200 °C).[7] This is really advantageous as it allows to regenerate the H-bonding in solid state after solution processes. This technique was used for the in-situ regeneration of an insoluble pigment in the solid/solvent medium by thermal treatment.[7b, 8]

On the other hand, triazatruxene (TAT) is a flat but soluble conjugated core made of three fused carbazole units and a good electron-donor as well. It has been recently demonstrated that dumbbell-shaped molecules using TAT units as π-stacking platforms and a central DPP unit as chromophore is a suitable design towards highly efficient organic small-molecules for OPV.[9] We therefore designed a dumbbell-shaped molecule (***t*-Boc-TATDPP**) based on *t*-Boc protected thiophene-diketopyrrolopyrole moiety (TDDP, **1**) as a core molecule and triazatruxene (TAT) attached at both sides of the DPP core. Thus it was anticipated that in ***t*-Boc-TATDPP**, the TAT units will promote the molecular self-assembling properties by enhancing the molecule π-π stacking ability while the long-alkyl chains and *t*-Boc groups will increase the molecule solubility in order to obtain high quality films from solution. After annealing at 200 °C, *t*-Boc groups will be removed to regenerate the hydrogen-bond network which is expected to further strengthen the intermolecular interactions in the films leading to an improvement of the charge transport properties of the DPP-based molecule and of the thin film morphology stability. This technique makes easy to process the films of H-bonded molecules with vacuum evaporation and

[a] Dr. S. Mula, Dr. N. Leclerc, Dr. G. Ulrich
Institut de chimie et procédés pour l'énergie, l'environnement et la santé (ICPEES), UMR CNRS 7515, Ecole Européenne de Chimie, Polymères et Matériaux (ECPM), 25 Rue Becquerel, Strasbourg 67087 Cedex 2, France.
E-mail: smula@barc.gov.in (SM); leclercn@unistra.fr (NL); gulrich@unistra.fr (GU)
[b] Bio-Organic Division, Bhabha Atomic Research Centre, Mumbai 400085, India.
[c] Homi Bhabha National Institute, Anushakti Nagar, Mumbai 400094, India.
[d] Dr. T. Han, Dr. T. Heiser, Dr. P. Lévêque
Le laboratoire des sciences de l'ingénieur, de l'informatique et de l'imagerie (ICube), UMR7357, Université de Strasbourg-CNRS, 23 rue du Loess, 67037 Strasbourg, France.
[e] A. P. Srivastava
Mechanical Metallurgy Division, Bhabha Atomic Research Centre, Mumbai 400085, India.
[f] Dr. A. Ruiz-Carretero
Institut Charles Sadron CNRS - UPR 22, 23 rue du Loess, Strasbourg 67034 Cedex 2, France.

Supporting information for this article is given via a link at the end of the document.

10.1002/chem.201900689

would be very important for the device developments which is explored here. The formation of the H-bonded supramolecular network was investigated thoroughly by measuring and comparing the UV-visible, IR and X-Ray diffraction spectra, and HR-TEM image of the ***t*-Boc-TATDPP** and its annealed thin films. Finally, the charge transport properties were measured and interestingly it was observed that the H-bonded supramolecular architecture has higher (2 orders of magnitude) hole mobility than ***t*-Boc-TATDPP**. Morphology robustness was also checked by using ***t*-Boc-TATDPP** as electron-donor in a blend with $PC_{71}BM$ as electron-acceptor in annealed condition. All the results were explained and rationalised by theoretical calculations and dedicated analysis.

Results and Discussion

Synthesis. For the synthesis of ***t*-Boc-TATDPP**, *t*-Boc protected TDPP, **1**,[7b] was reacted with NBS to furnish 2,2'-dibromo-N,N-di-*t*-Boc TDPP (**2**) in good yield. 2-Boronate-N,N,N-trihexyl-5,10,15-triazatruxene (**4**) was synthesized by *n*-BuLi promoted reaction of 2-bromo-N,N,N-trihexyl-5,10,15-triazatruxene (**3**)[10] and 2-isopropoxy-4,4,5,5-tetramethyl-1,3,2-dioxaborolane. Then the Suzuki−Miyuara coupling reaction of **2** with **4** afforded ***t*-Boc-TATDPP** (Scheme 1). All these compounds were purified by flash chromatography and characterized by NMR spectroscopy.

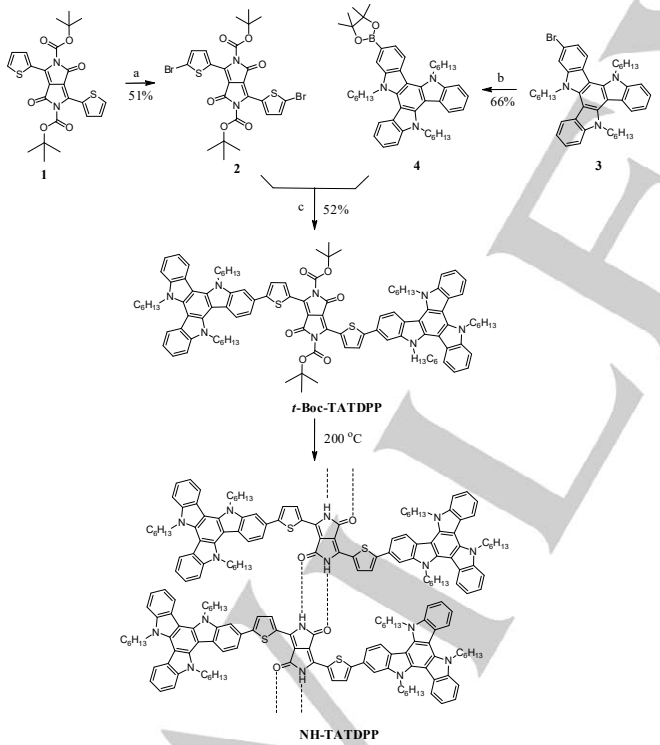

Scheme 1. Synthesis of compound ***t*-Boc-TATDPP** and **NH-TATDPP**. a) NBS, $CHCl_3$, 25 °C, 24 h. b) *n*-BuLi, 2-Isopropoxy-4,4,5,5-tetramethyl-1,3,2-dioxaborolane, THF, -78 °C, 2 h. c) $Pd(PPh_3)_4$, K_2CO_3, dioxane, 55 °C, 16 h.

In thermogravimetric analysis (TGA), after heating at 200 °C, the *t*-Boc groups of ***t*-Boc-TATDPP** were removed in agreement with the observed weight-loss closed to the theoretical one (ca 12%) around 200 °C (Figure 1). This was also confirmed by NMR and mass spectroscopy. In ^1H NMR spectrum (Figure S3), the disappearance of the singlet attributed to the methyl protons of the *t*-Boc groups at 1.67 ppm and the appearance of a singlet at 10.90 ppm corresponding to the two amide N-H protons confirmed the removal of the *t*-Boc groups and the synthesis of **NH-TATDPP**. Further, in the MALDI-TOF experiment, a molecular ion peak corresponding to **NH-TATDPP** was obtained (Figure S4). Thus a thermal-annealing at a temperature ≥ 200 °C will regenerate the NH groups (**NH-TATDPP**) and should strengthen the intermolecular interactions by forming intermolecular H-bonding with the neighbouring molecules from both sides (Scheme 1). The array of H-bonded molecules became insoluble in common organic solvents.[7b, 8b]

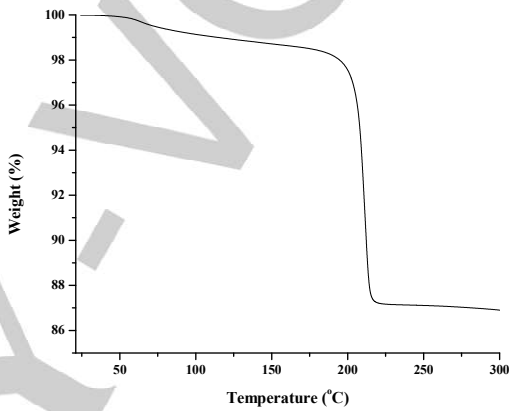

Figure 1. Thermogravimetric analysis (TGA) of ***t*-Boc-TATDPP**.

Photophysical properties. The photophysical properties of the **TDDP**, **1** in dichloromethane (CH_2Cl_2) were evaluated at room temperature (25 °C) (Table 1). Figure 2 shows the absorption, emission and excitation spectra of **1** in CH_2Cl_2. Compound **1** showed one broad band with the longest wavelength absorption maximum (λ_{max}) ($S_0 \rightarrow S_1$ absorption band) located at 484 nm (Table 1), a typical absorption spectrum of DPP dyes. The dye was moderately fluorescent (Φ_{fl} = 29 %) with λ_{em} at 538 and 586 nm.

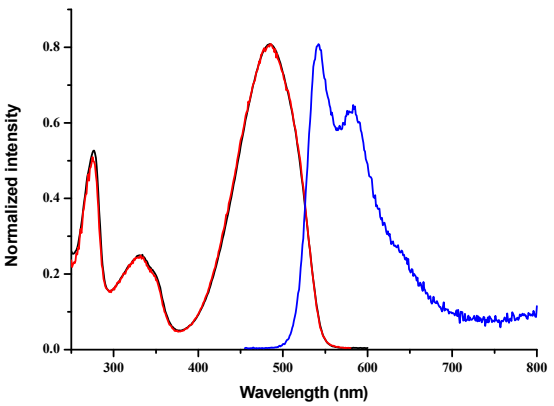

Figure 2. Normalized absorption (black), fluorescence (blue) and excitation (red) spectra of TDDP, **1**.

Table 1. Selected optical properties of compounds **1**, ***t*-Boc-TATDPP** and **NH-TATDPP**.

Compounds	UV-vis Absorption			
	Solution (CH_2Cl_2)	Film		
	λ_{abs} [nm]	λ_{abs} [nm]	λ_{onset} [nm]	Eg_{opt} (eV)
1	484	-	-	-
***t*-Boc-TATDPP**	632, 319	712, 640, 331	792	1.57
NH-TATDPP	613[a]	680, 620, 323	737	1.68

[a] In $CHCl_3$ and MeOH mixture.

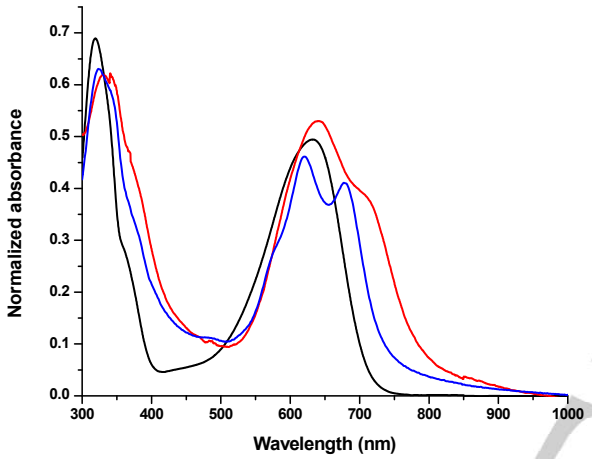

Figure 3. Normalized absorption spectra of ***t*-Boc-TATDPP** in CH_2Cl_2 (black) and thin film (red) and, its thermally treated film i.e. thin film of **NH-TATDPP** (blue).

The UV-vis absorption spectra of ***t*-Boc-TATDPP** in CH_2Cl_2 and thin film are shown in Figure 3. The spectrum corresponding to a thermally annealed film at a temperature of 200 °C *i.e.* a **NH-TATDPP** thin film is also shown in Figure 3. Thin film of ***t*-Boc-TATDPP** was prepared by drop-casting from its $CHCl_3$ solution (<0.4 wt %) on a quartz plate. This film was heated at 200 °C for 30 min. in air on a hot plate to prepare the thermally treated film i.e. thin film of **NH-TATDPP**. In solution, the absorption band of ***t*-Boc-TATDPP** is highly (148 nm) red-shifted with λ_{max} at 632 nm as compared to compound **1** (Table 1). This indicates the planar structure of this molecule with extended conjugation within the central DPP core and lateral TAT units. The planar structure of the molecule is also confirmed by theoretical calculation explained *vide infra*. The compound was completely non-fluorescent. In thin film, due to the strengthening of the intermolecular π-π stacking in the solid-state, the absorption band of ***t*-Boc-TATDPP** was further red-shifted with λ_{max} at 640 nm and a shoulder peak at 712 nm (Table 1, Figure 3) appear which could be attributed to excitonic coupling by aggregation in solid state.[11] After annealing, both peaks were sharpended and blue shifted to 620 and 680 nm, respectively, due to rigidification of the solid state arrangement and probable limitation of the number of possible interactions. The onset wavelength value was also blue-shifted by approximately 55 nm. This blue shift observed for **NH-TATDPP** could come from either the change in the frontier molecular orbitals after *t*-Boc elimination (rising of the LUMO level) and/or from a twist in the conjugation backbone resulting from the H-bonding creation. Similar effects were observed in previous studies with annealed thin films based on donor-acceptor type DPP-based small molecules as compared to their un-annealed thin films.[7b, 8b, 12] The optical energy gaps (Eg_{opt}) estimated from the onset wavelength of ***t*-Boc-TATDPP** and **NH-TATDPP** films were 1.57 and 1.68 eV, respectively (Table 1).

The presence of H-bonding in solution of **NH-TATDPP** was investigated through an in-depth UV/Vis study. Unfortunately, **NH-TATDPP** was insoluble in non-polar solvents.[7, 8b] It was merely soluble in chloroform ($CHCl_3$), which showed an absorption band at 636 nm with a shoulder peak at 613 nm (Figures S5 and S6). A hypsochromic shift is observed as compared to absorption spectra of **NH-TATDPP** in thin film as also seen in case of ***t*-Boc-TATDPP** (Figure S5). This is a consequence of stronger intermolecular interactions in the solid state. After gradual addition of methanol (MeOH), a H-bond-disrupting protic solvent, the absorption peak intensity at 636 nm decreased while the absorption intensity at 613 nm increased gradually (Figure S6). This clearly indicated that the peak at 636 nm corresponds to H-aggregation of **NH-TATDPP**.[2d, 13] In contrast ***t*-Boc-TATDPP** exhibited no change in the absorption spectra in $CHCl_3$ even after addition of a large amount of MeOH and therefore confirmed the important role of H-bonding between the amide groups for the self-assembly of **NH-TATDPP**.

Solid state properties. Removal of the *t*-Boc groups upon thermal treatment of ***t*-Boc-TATDPP** to regenerate the NH groups and formation of the hydrogen bonds of N-H···O=C in **NH-TATDPP** (Scheme 1) was clearly evidenced from IR spectroscopic analysis. IR spectra of ***t*-Boc-TATDPP** showed two peaks for free-carbonyl stretching vibration of the *t*-Boc and DPP core at 1744 and 1675 cm^{-1}, respectively (green arrows in Figure 4). Both peaks disappeared after annealing at 200 °C for 30 min and the characteristic peak for the hydrogen-bonded carbonyl groups was found at 1632 cm^{-1}. Moreover, a broad peak due to the regenerated NH groups was also observed between 2600 and 3200 cm^{-1} (Figure 4).[7b] These results confirmed the formation of hydrogen-bonded network in **NH-TATDPP**.

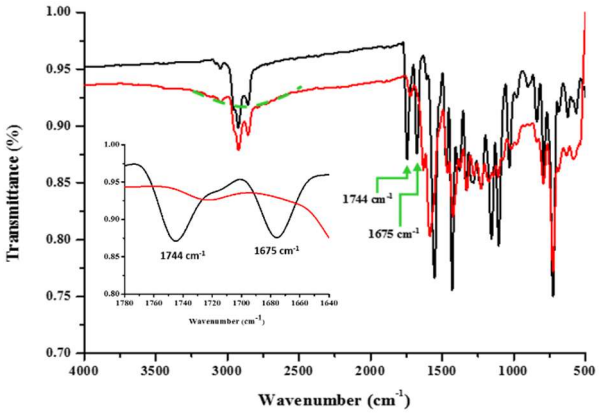

Figure 4. IR spectra of ***t*-Boc-TATDPP** (black) and its thermally treated compound, **NH-TATDPP** (red).

Then, XRD experiments were performed on ***t*-Boc-TATDPP** and its thermally treated compound **NH-TATDPP** thin-films. Those experiments were carried-out to check the crystallinity and the ordering of the compounds in thin films before and after thermal cleavage of the *t*-Boc groups as shown in Figure 5a. The thin-film of ***t*-Boc-TATDPP** for XRD analysis was prepared by drop-casting from a CH_2Cl_2 solution (10 mg ml^{-1}) on a glass plate which was heated at 200 °C for 30 min to prepare the thin film of **NH-TATDPP**. The casted film of ***t*-Boc-TATDPP** showed a peak at 2θ = 5.413° which corresponds to a d-spacing of 1.63 nm. This peak reflected the alkyl-chain stacking in the thin film. No peak was found related to π–π intermolecular stacking interactions. However, the thermally treated thin film showed a shift in alkyl-chain staking peak with a simultaneous increase in peak intensity. Also, a new peak appeared at 2θ = 29.55° which corresponds to a d-spacing of 0.30 nm (Figure 5a). All these changes indicate an improvement in the crystallinity of the film resulting from strong intermolecular interactions due to N–H···O=C H-bonding and strong π–π stacking between molecules (Figure 5b). This was possible due to the reduction in steric hindrance when the bulky *t*-Boc groups are thermally cleaved at 200 °C. This supports the observation mentioned in the IR studies. In addition, it means that the blue shift observed in the solid-state absorption after annealing (Figure 3) is probably more correlated to the frontier molecular orbital modification upon electron withdrawing *t*-Boc de-protection.

Further, HR-TEM images are collected to confirm the crystalline structure of the **NH-TATDPP** film due to H-bonding and π–π stacking as indicated by X-ray diffraction pattern (Figure 5c-d).[8b, 14] The HR-TEM images showed long-range ordered structure of **NH-TATDPP** with d-spacing of 0.30 nm which perfectly matches with the XRD analysis result. This also confirmed the π–π stacked structure of **NH-TATDPP** (Figure 5b).[8b, 14a]

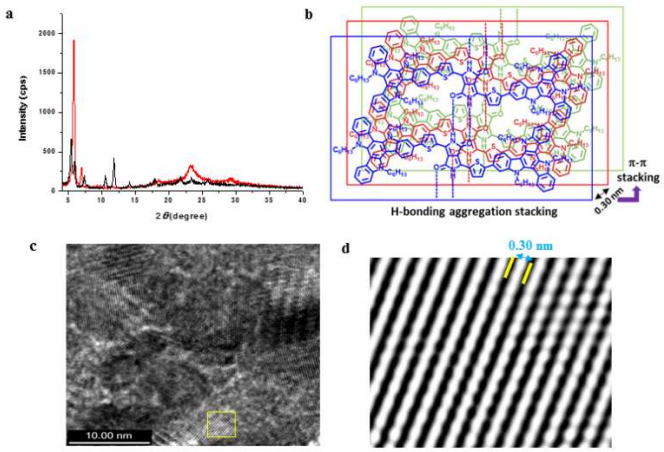

Figure 5. (a) X-ray diffraction patterns for ***t*-Boc-TATDPP** (black) and **NH-TATDPP** (red). (b) Schematic illustration of the proposed chemical arrangement of NH-TATDPP. (c) HR-TEM image of NH-TATDPP after thermal annealing. (d) Processed image from the square part of (c).

Cyclic voltammetry. The oxidation and reduction processes of ***t*-Boc-TATDPP** were investigated by cyclic voltammetry (CV) experiments done in CH_2Cl_2 solution. The energies of its highest occupied molecular orbital (HOMO) and lowest unoccupied molecular orbital (LUMO) levels were also determined from the redox data.

The pure compound ***t*-Boc-TATDPP** displayed one reversible and one non-reversible reduction waves at -1.04 V and -1.68 V respectively, which appeared due to reduction of the DPP-thienyl central core (Figure 6, Table 2). The TAT fragment is not electroactive in reduction but easily oxidizable. It exhibited two reversible mono electronic oxidations at +0.75 V and + 1.28 V.[15] The DPP exhibited two reversible oxidation waves, at +0.56 V and +1.04 V as confirmed by comparing with the model compounds (Figure 6, Table 2). The HOMO and LUMO energies calculated from CV are -5.32 eV and -3.72 eV respectively (Table 2). The HOMO-LUMO energy gap (1.60 eV), measured from electrochemical measurement, is in line with the optical gap (1.57 eV) determined form the thin film absorption spectra (Table 1). Most importantly, all these energy data clearly indicated that ***t*-Boc-TATDPP** can be used as a good electron-donor when blended with the electron-acceptor $PC_{71}BM$ (Figure 7).

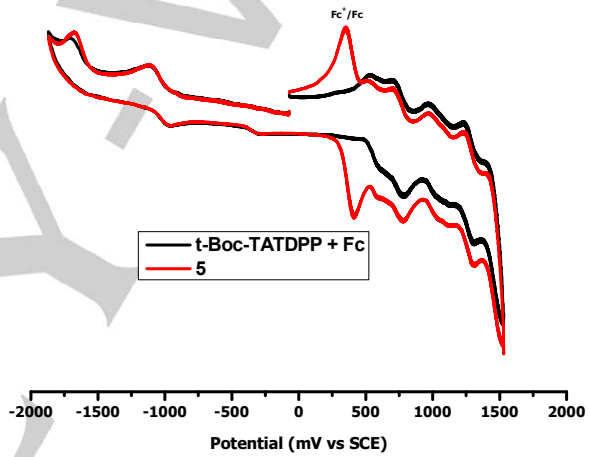

Figure 6. Cyclic voltammogram of compound ***t*-Boc-TATDPP** in CH_2Cl_2 containing 0.1 M tetrabutylammonium hexafluorophosphate at 25 °C. Potentials were calibrated versus the saturated calomel electrode (SCE), using the ferrocene/ferrocinium (Fc/Fc^+) couple as an internal reference and a conventional scan rate of 150 mV/s.

Table 2. Electrochemical properties of ***t*-Boc-TATDPP** in CH_2Cl_2 (3×10^{-3} M) at 25 °C.[a]

Compound	E_{ox}°/V	E_{red}°/V	HOMO (eV)	LUMO (eV)	Band Gap (eV)
***t*-Boc-TATDPP**	+ 0.56 + 0.75 + 1.04 + 1.28	-1.04 -1.68 (irr)	-5.32	-3.72	1.60

[a] The error in half-wave potentials is ±10 mV.

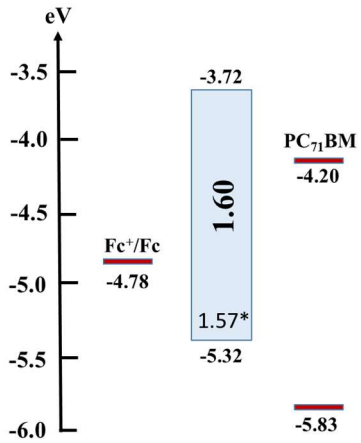

Figure 7. HOMO/LUMO energy levels for ***t*-Boc-TATDPP**, ferrocene and $PC_{71}BM$[9a] as determined by electrochemistry. Optical gap (∗) was determined form the thin film absorption spectra.

Theoretical calculations. The minimal energy configuration of compound ***t*-Boc-TATDPP** was optimized to understand its ground state geometry and also to visualize and calculate the energies of its HOMO and LUMO. Anticipating no influence of the hexyl chains on its electronic structures, all the hexyl side chains of the TAT units of ***t*-Boc-TATDPP** were replaced by methyl groups to shorten the calculation time.

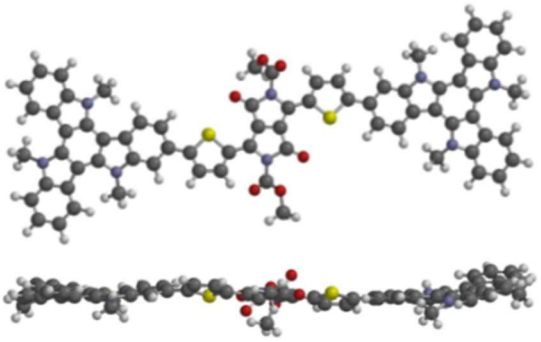

Figure 8. Optimized structure of ***t*-Boc-TATDPP** from two different view angles.

The optimized structure of ***t*-Boc-TATDPP** (Figure 8) clearly shows that the molecule is rather planar as visible from two different view angles. The HOMO and LUMO levels and their spatial extend were also calculated. The calculated HOMO and LUMO surfaces are shown in Figure 9. The LUMO is mainly confined to the central DPP unit. But the HOMO spreads significantly over the central DPP core and the two TAT moieties. The calculated frontier energy levels for the LUMO and HOMO are -2.67 eV and -4.72 eV, respectively. The calculated HOMO energy is reasonably close to the measured (by CV) HOMO energy (-5.32 eV) but the calculated LUMO energy is 1.05 eV higher than the one measured by CV (-3.72 eV). This is a common observation for this type of calculations.[16]

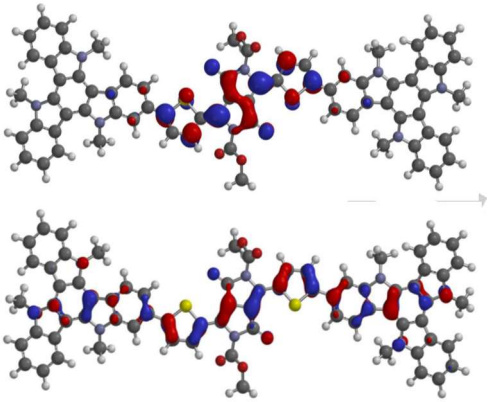

Figure 9. Calculated LUMO (top) and HOMO (bottom) surfaces of compound ***t*-Boc-TATDPP**.

In order to understand the different extension of the frontier energy level surfaces, the minimal energy configuration of the central DPP trimer and of the TAT moiety were optimized separately and their HOMO and LUMO energies were calculated. The calculated HOMO and LUMO surfaces are shown in Figure 10-11 and their respective energies are given in Table 3. The LUMO of the TAT and of the central DPP dye are far away in an energetic point of view (almost 2.5 eV difference) (Table 3) and therefore only limited hybridization can take place and the LUMO of the dumbbell-shaped molecule is very close to the LUMO of the central DPP dye, both in shape and energy value (-2.67 eV for ***t*-Boc-TATDPP** and -2.98 eV for the central DPP dye). The situation is different for the HOMO as the TAT HOMO (-4.94 eV) is rather close in energy to the central DPP dye HOMO (-5.61 eV) (Table 3). Hybridization can take place and as a result the HOMO of ***t*-Boc-TATDPP** is a combination of the HOMO of both moieties and is shallower in energy than the shallowest HOMO (the TAT HOMO). Thus, the DFT on the moieties is consistent with the calculations on ***t*-Boc-TATDPP**. It should be noted that hybridization of the frontier energy levels could also be hindered by an important dihedral angle between the moieties. It is obviously not the case here with a planar dumbbell-shape molecule (Figure 8).

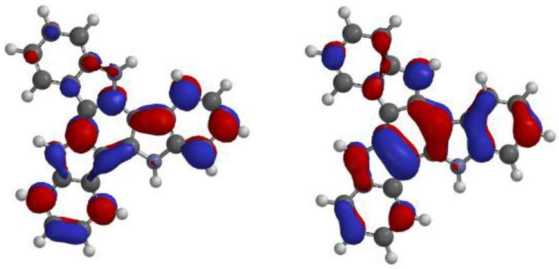

Figure 10. Calculated LUMO (left) and HOMO (right) surfaces of TAT moiety.

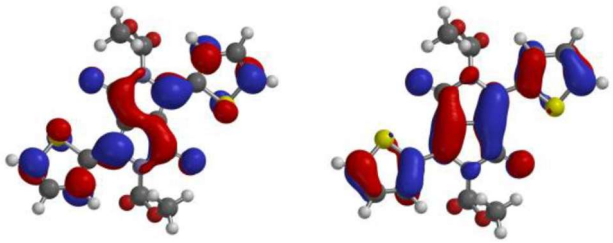

Figure 11. Calculated LUMO (left) and HOMO (right) surfaces of DPP moiety.

Table 3. Calculated HOMO and LUMO energy levels of ***t*-Boc-TATDPP** (second column), DPP (third column) and TAT unit (fourth column).

Dye	***t*-Boc-TATDPP**	DPP unit	TAT unit
$HOMO_{DFT}$ (eV)	-4.72 eV	-5.61 eV	-4.94 eV
$LUMO_{DFT}$ (eV)	-2.67 eV	-2.98 eV	-0.50 eV

Charge transport properties. Charge transport properties of pure compounds ***t*-Boc-TATDPP** and **NH-TATDPP** were measured using organic field-effect transistors (O-FETs) in the bottom-gate top-contact configuration (Table 4). When ***t*-Boc-TATDPP** is used as OFET semiconducting channel, the measured hole OFET mobility is rather low ($2.4x10^{-5}$ $cm^2V^{-1}s^{-1}$) which is further decreased by factor of 7 ($3.4x10^{-6}$ $cm^2V^{-1}s^{-1}$) after the first thermal-annealing step at 110 °C. Interestingly, after the second annealing at 200 °C *i.e.* when *t*-Boc protecting group were removed and the H-bonded network was created (*i.e.* **NH-TATDPP** is the OFET channel), a strong increase (124 times) of the hole mobility ($4.2x10^{-4}$ $cm^2V^{-1}s^{-1}$) is measured (Figure 12-14). As expected, the measured hole mobility is unchanged after further annealing of the compound at 230 °C as H-bonded network was already formed after annealing at 200 °C. Previous reports showed that the insulating substituents (alkyl, *t*-Boc) at the amide N-atom of DPP dyes have very weak/no influence on the charge transport properties of DPP based molecules.[7b, 8b, 17] These also support our observation that the increase in hole mobility of **NH-TATDPP** is only due to the supramolecular architecture formation.

Table 4. Charge transport properties of ***t*-Boc-TATDPP** and **NH-TATDPP**.

Sample	**Hole Mobility** ($cm^2V^{-1}s^{-1}$)
***t*-Boc-TATDPP** (at 25 °C)	$2.4x10^{-5}$
***t*-Boc-TATDPP** (at 110°C)	$3.4x10^{-6}$
NH-TATDPP (at 200 or 230 °C)	$4.2x10^{-4}$
***t*-Boc-TATDPP**/$PC_{71}BM$ (at 25 °C)	$5.5x10^{-6}$
***t*-Boc-TATDPP**/$PC_{71}BM$ (at 110 °C)	$1.0x10^{-6}$
NH-TATDPP/$PC_{71}BM$ (at 200 or 230 °C)	$4.2x10^{-4}$

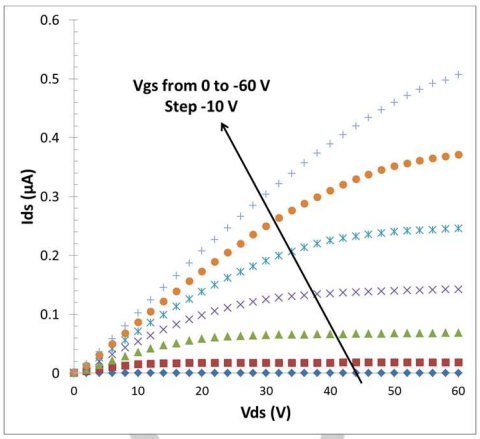

Figure 12. Output characteristic of a as-deposited hole-only ***t*-Boc-TATDPP** OFET.

Output characteristics of as deposited ***t*-Boc-TATDPP** transistors i.e. the drain-source current (Ids) as a function of the drain-source voltage (Vds) for increasing values of the gate voltage (Vgs) are shown in Figure 12. The characteristics correspond to hole-only OFETs with negative values for Ids, Vds and Vgs. The corresponding transfer characteristics in the saturation regime i.e. Ids as a function of Vgs for a fixed -60V Vds value are shown in Figure 14. The output characteristics of the same OFET annealed subsequently at 110 °C for 10 minutes, 200 °C for 10 minutes and 230 °C for 15 minutes are shown in Figure 13 which corresponds to a hole-only OFET whose channel is made of **NH-TATDPP**. The corresponding transfer characteristics are also represented in Figure 14.

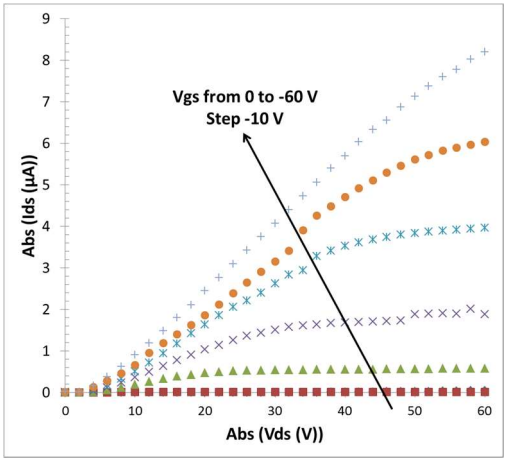

Figure 13. Output characteristic of a hole-only **NH-TATDPP** OFET.

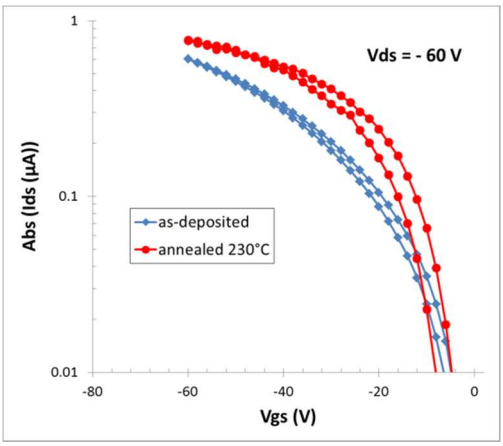

Figure 14. Transfer characteristics in the saturation regime of a as-deposited hole-only ***t*-Boc-TATDPP** OFET (blue) and its corresponding **NH-TATDPP** OFET (red).

Next, charge transport properties of blends of ***t*-Boc-TATDPP** and $PC_{71}BM$ and, **NH-TATDPP** and $PC_{71}BM$ were measured by using both blends as semiconducting channel in field-effect transistors. Hole mobility of ***t*-Boc-TATDPP** in the presence of $PC_{71}BM$ ($5.5x10^{-6}$ $cm^2V^{-1}s^{-1}$) was 4 times lower than that of pure ***t*-Boc-TATDPP**. After the annealing at 200 °C i.e. when NH-TATDPP is formed, blends of **NH-TATDPP**/$PC_{71}BM$ showed a strong increase of the hole mobility ($4.2x10^{-4}$ $cm^2V^{-1}s^{-1}$). As expected, no change in hole mobility was observed after further annealing at 230 °C. The fact that **NH-TATDPP** showed similar hole mobilities in pure compound and in blends with $PC_{71}BM$ is a clear signature of the morphology robustness when using **NH-TATDPP** as electron-donor in blend with $PC_{71}BM$ as electron-acceptor. This property could be useful for its further use in the fabrication of organic solar cells as the active-layer morphology robustness is a key-parameter for photovoltaic performances stability.

Conclusions

Thus, a highly soluble dumbbell-shaped molecule, ***t*-Boc-TATDPP** based on *t*-Boc protected thiophene-DPP and triazatruxene (TAT) moieties was synthesized. After surface deposition the two *t*-Boc groups of the molecule were removed by annealing at 200 °C which created a supramolecular network with H-bonded network of **NH-TATDPP** supported by additional π-π stacking. The H-bonded network formation by thermal-annealing was characterised by various methods like TGA, UV-vis, IR, XRD and HR-TEM measurements. Further, FETs were fabricated with a semiconducting channel made of ***t*-Boc-TATDPP** and **NH-TATDPP**. It was noticed that **NH-TATDPP** showed significantly higher (124 times) hole mobilities compared to ***t*-Boc-TATDPP**. Further, this high hole mobility in the case of **NH-TATDPP** was unaffected upon blending with $PC_{71}BM$. These observations are consistent with the hypothesis that a supramolecular organization based on hydrogen bonds between NH groups and adjacent carbonyl groups give highly ordered and robust molecular arrangements in thin-films. All these observations are encouraging for using this supramolecular approach for enhancing efficiency and stability of organic optoelectronic devices.

Experimental Section

General procedure for synthesis of Di-*tert*-butyl 3,6-Bis-(5-bromo-thiophen-2-yl)-1,4-dioxopyrrolo[3,4-c]pyrrole-2,5-dicarboxylate (2).[7b] To a solution of di-*tert*-butyl 1,4-dioxo-3,6-di(thiophen-2-yl)pyrrolo-[3,4-c]pyrrole-2,5-dicarboxylate (**1**) (150 mg, 0.30 mmol) in $CHCl_3$ (15 mL), N-bromosuccinimide (NBS) (117 mg, 0.66 mmol) was added and the mixture was stirred for 24 h at 25 °C. Then, the organic layer was washed with H_2O (3 X 10 mL) and dried over anhydrous Na_2SO_4. After removal of the solvent under vacuum, the residue was purified by column chromatography (silica gel, CH_2Cl_2/PE, 50:50) to furnish pure **2** (101 mg, 51%) as red solid. ^1H NMR (300 MHz, $CDCl_3$, 25 °C, TMS): δ 1.62 (s, 18H), 7.16 (d, *J* = 4.2 Hz, 2H), 8.08 (d, *J* = 4.2 Hz, 2H). ^{13}C NMR (75 MHz, $CDCl_3$, 25 °C, TMS): δ 27.9, 29.8, 86.5, 110.4, 121.0, 131.0, 131.2, 135.6, 136.8, 148.9, 158.7.

General procedure for synthesis of compound 4.[18] To a cooled (-78 °C) solution of **3** (500 mg, 0.74 mmol) in THF (25 mL), ^{n}BuLi (0.51 mL, 0.81 mmol) was added dropwise and the mixture was stirred for 1h. Then 2-isopropoxy-4,4,5,5-tetramethyl-1,3,2-dioxaborolane (165 mg, 0.89 mmol) was added to the mixture and stirred for another 1h. The mixture was warmed to room temperature, and the solvent was evaporated to dryness. The crude was dissolved in CH_2Cl_2 and was washed with water (3 X 30 mL) and dried over anhydrous Na_2SO_4. After removal of the solvent under vacuum, the residue was purified by column chromatography (silica gel, CH_2Cl_2/PE, 50:50) to furnish pure **4** (350 mg, 66%) as a colourless oil. ^1H NMR (300 MHz, $CDCl_3$, 25 °C, TMS): δ 0.85 (t, *J* = 7.6 Hz, 9H), 1.27-1.42 (m, 18H), 1.49 (s, 12H), 4.93 (t, *J* = 7.6 Hz, 4H), 5.03 (t, *J* = 7.6Hz, 2H), 7.35-7.41 (m, 2H), 7.46-7.51 (m, 2H), 7.66 (d, *J* = 7.9 Hz, 2H), 7.85 (d, *J* = 8.2 Hz, 1H), 8.15 (s, 1H), 8.31-8.34 (m, 3H); ^{13}C NMR (75 MHz, $CDCl_3$, 25 °C, TMS): δ 14.0, 22.5, 22.6, 22.7, 25.0, 25.1, 26.3, 26.4, 26.5, 29.8, 30.1, 31.4, 31.5,31.6, 46.9, 47.1, 83.8, 103.2, 103.3, 110.5, 117.1, 119.7, 120.8, 121.5, 121.7, 122.8, 123.4,123.5, 123.6, 126.1, 127.8, 131.4, 134.8, 138.9, 139.4, 139.7, 140.6, 141.0, 141.1. MS (m/z): 723.7 $[M]^+$.

General procedure for synthesis of compound *t*-Boc-TATDPP. A mixture of **2** (90 mg, 0.14 mmol), **4** (220.0 mg, 0.30 mmol), $Pd(PPh_3)_4$ (18 mg, 0.03 mmol) and K_2CO_3 (36 µL of 1M solution, 0.36 mmol) in dioxane/H_2O (10/1, v/v, 11 mL) in a Schlenk flask was degassed thoroughly and then stirred at 55 °C for 16 h under argon. Water (10 mL) was added to the reaction mixture and the mixture was extracted with CH_2Cl_2. The organic layer was dried over anhydrous Na_2SO_4. After removal of the solvent under vacuum, the residue was purified by column chromatography (silica gel, CH_2Cl_2/PE, 50:50) to furnish pure ***t*-Boc-TATDPP** (120 mg, 52%) as blue solid. ^1H NMR (400 MHz, C_6D_6, 60 °C, TMS): δ 0.68-0.74 (m, 18H), 1.00-1.14 (m, 36H), 1.67 (s, 18H), 1.78-1.83 (m, 12H), 4.77-4.83 (m, 12H), 7.38 (d, *J* = 4.1 Hz, 2H), 7.41-7.50 (m, 8H), 7.54-7.58 (m, 4H), 7.76 (dd, *J* = 8.4 Hz, 2H), 7.96 (d, *J* = 1.6 Hz, 2H), 8.33 (d, *J* = 8.5 Hz, 2H),8.40-8.46 (m, 4H), 8.79 (d, *J* = 4.1 Hz, 2H); ^{13}C NMR (100 MHz, C_6d_6, 60°C, TMS): δ 13.8, 13.9, 14.0, 22.6, 22.7, 26.5, 26.6, 28.0, 29.8, 29.9, 31.5, 31.6, 31.7, 47.4, 84.9, 104.5, 104.7,108.8, 110.8, 111.2, 111.3, 119.0, 120.3, 120.4, 122.4, 122.6, 123.4, 124.1, 124.3, 124.4, 125.0, 127.4, 128.7, 136.3, 136.9, 139.4, 140.1, 140.7, 142.0, 142.1, 142.3, 150.2, 152.6, 159.4; MALDI-TOF (m/z): 1691.777 $[M+1]^+$; Anal. calcd. for $C_{108}H_{122}N_8O_6S_2$: C, 76.65; H, 7.27; N, 6.62%. Found: C, 76.97; H, 7.13; N, 6.81%.

NH-TATDPP. ^1H NMR (600 MHz, $(CD_3)_2SO$, 110 °C, TMS): δ 0.65-0.69 (m, 18H), 1.05-1.12 (m, 36H), 1.76-1.78 (m, 12H), 4.99-5.03 (dt, 8H), 5.10 (t, *J* = 7.1 Hz, 4H), 7.38 (q, *J* = 7.5 Hz, 4H), 7.49 (t, *J* = 7.5 Hz, 4H), 7.73 (d, *J* = 8.3 Hz, 2H), 7.80-7.84 (m, 6H), 8.14 (s, 2H), 8.31-8.38 (m, 8H), 10.90 (s, 2H); MALDI-TOF (m/z): 1490.476 $[M]^+$.

Acknowledgements

S.M. is thankful to French National Agency (ORION project ANR-13-PRGE-0001) for the financial support and to BARC for giving permission for conducting research in ECPM, Strasbourg.

Keywords: Supramolecular chemistry • Dyes/Pigments • Hydrogen-bond • Organic semiconductor • OFET

[1] a) J. M. Lehn, *Supramolecular Chemistry: Concepts and Perspectives*, John Wiley & Sons, **2011**; b) J.-M. Lehn, *Angew. Chem. Int. Ed.* **2013**, *52*, 2836-2850; c) A. Sikder, D. Ray, V. K. Aswal, S. Ghosh, *Angew. Chem. Int. Ed.* **2019**, *58*, 1606-1611.

[2] a) H. Zhang, K. Liu, K.-Y. Wu, Y.-M. Chen, R. Deng, X. Li, H. Jin, S. Li, S. S. C. Chuang, C.-L. Wang, Y. Zhu, *J. Phys. Chem. C* **2018**, *122*, 5888-5895; b) G. H. Roche, Y.-T. Tsai, S. Clevers, D. Thuau, F. Castet, Y. H. Geerts, J. J. E. Moreau, G. Wantz, O. J. Dautel, *J. Mater. Chem. C* **2016**, *4*, 6742-6749; c) M. U. Ocheje, B. P. Charron, Y.-H. Cheng, C.-H. Chuang, A. Soldera, Y.-C. Chiu, S. Rondeau-Gagné, *Macromolecules* **2018**, *51*, 1336-1344; d) M. R. Molla, D. Gehrig, L. Roy, V. Kamm, A. Paul, F. Laquai, S. Ghosh, *Chem. Eur. J* **2014**, *20*, 760-771; e) S. Ghosh, S. Das, A. Saeki, V. K. Praveen, S. Seki, A. Ajayaghosh, *ChemNanoMat* **2018**, *4*, 831-836; f) D. Basak, D. S. Pal, T. Sakurai, S. Yoneda, S. Seki, S. Ghosh, *Phys. Chem. Chem. Phys.* **2017**, *19*, 31024-31029; g) X. Lin, M. Suzuki, M. Gushiken, M. Yamauchi, T. Karatsu, T. Kizaki, Y. Tani, K.-i. Nakayama, M. Suzuki, H. Yamada, T. Kajitani, T. Fukushima, Y. Kikkawa, S. Yagai, *Sci. Rep.* **2017**, *7*, 43098.

[3] a) Y. D. Park, J. K. Park, J. H. Seo, J. D. Yuen, W. H. Lee, K. Cho, G. C. Bazan, *Adv. Energy Mater.* **2010**, *1*, 63-67; b) K.-H. Kim, H. Yu, H. Kang, D. J. Kang, C.-H. Cho, H.-H. Cho, J. H. Oh, B. J. Kim, *J. Mater. Chem. A* **2013**, *1*, 14538-14547; c) S. Park, B. T. Lim, B. Kim, H. J. Son, D. S. Chung, *Sci. Rep.* **2014**, *4*, 5482.

[4] O. Wallquist, R. Lenz, *Macromol Symp.* **2002**, *187*, 617-630.

[5] a) Y. Qiao, Y. Guo, C. Yu, F. Zhang, W. Xu, Y. Liu, D. Zhu, *J. Am. Chem. Soc.* **2012**, *134*, 4084-4087; b) B. Lim, H. Sun, J. Lee, Y.-Y. Noh, *Sci. Rep.* **2017**, *7*, 164; c) Z. Chen, M. J. Lee, R. Shahid Ashraf, Y. Gu, S. Albert-Seifried, M. Meedom Nielsen, B. Schroeder, T. D. Anthopoulos, M. Heeney, I. McCulloch, H. Sirringhaus, *Adv. Mater.* **2011**, *24*, 647-652; d) J. D. Yuen, J. Fan, J. Seifter, B. Lim, R. Hufschmid, A. J. Heeger, F. Wudl, *J. Am. Chem. Soc.* **2011**, *133*, 20799-20807; e) A. R. Mohebbi, J. Yuen, J. Fan, C. Munoz, M. f. Wang, R. S. Shirazi, J. Seifter, F. Wudl, *Adv. Mater.* **2011**, *23*, 4644-4648; f) P.-T. Wu, F. S. Kim, S. A. Jenekhe, *Chem. Mater.* **2011**, *23*, 4618-4624; g) T. Bura, S. Beaupré, O. A. Ibraikulov, M.-A. Légaré, J. Quinn, P. Lévêque, T. Heiser, Y. Li, N. Leclerc, M. Leclerc, *Macromolecules* **2017**, *50*, 7080-7090; h) Y.-F. Huang, S.-T. Chang, K.-Y. Wu, S.-L. Wu, G.-T. Ciou, C.-Y. Chen, C.-L. Liu, C.-L. Wang, *ACS Appl. Mater. Interfaces* **2018**, *10*, 8869-8876; i) Y. Suna, J.-i. Nishida, Y. Fujisaki, Y. Yamashita, *Chem. Lett.* **2011**, *40*, 822-824.

[6] S. Qu, H. Tian, *Chem. Commun.* **2012**, *48*, 3039-3051.

[7] a) J. S. Zambounis, Z. Hao, A. Iqbal, *Nature* **1997**, *388*, 131; b) Y. Suna, J.-i. Nishida, Y. Fujisaki, Y. Yamashita, *Org. Lett.* **2012**, *14*, 3356-3359.

[8] a) Y. Hiroyuki, M. Jin, A. Shinji, S. Yoshimasa, *Jpn. J. Appl. Phys.* **2008**, *47*, 4728; b) C. K. Trinh, H.-J. Lee, J. W. Choi, M. Shaker, W. Kim, J.-S. Lee, *New J. Chem.* **2018**, *42*, 2557-2563.

[9] a) T. Bura, N. Leclerc, R. Bechara, P. Lévêque, T. Heiser, R. Ziessel, *Adv. Energy Mater.* **2013**, *3*, 1118-1124; b) I. Bulut, P. Chávez, A. Mirloup, Q. Huaulmé, A. Hébraud, B. Heinrich, S. Fall, S. Méry, R. Ziessel, T. Heiser, P. Lévêque, N. Leclerc, *J. Mater. Chem. C* **2016**, *4*, 4296-4303.

[10] a) C. Ruiz, J. T. López Navarrete, M. C. Ruiz Delgado, B. Gómez-Lor, *Org. Lett.* **2015**, *17*, 2258-2261; b) I. Bulut, Q. Huaulmé, A. Mirloup, P. Chávez, S. Fall, A. Hébraud, S. Méry, B. Heinrich, T. Heiser, P. Lévêque, N. Leclerc, *ChemSusChem* **2017**, *10*, 1878-1882.

[11] N. J. Hestand, F. C. Spano, *Acc. Chem. Res.* **2017**, *50*, 341-350.

[12] C. Liu, S. Dong, P. Cai, P. Liu, S. Liu, J. Chen, F. Liu, L. Ying, T. P. Russell, F. Huang, Y. Cao, *ACS Appl. Mater. Interfaces* **2015**, *7*, 9038-9051.

[13] S. Militzer, T. M. P. Tran, P. J. Mésini, A. Ruiz-Carretero, *ChemNanoMat* **2018**, *4*, 790-795.

[14] a) H.-J. Lee, S.-O. Hur, M.-K. Ahn, M. Changez, J.-S. Lee, *Nanoscale* **2017**, *9*, 6545-6550; b) R. F. Egerton, P. Li, M. Malac, *Micron* **2004**, *35*, 399-409; c) M. H. Loretto, R. E. Smallman, *Mater. Sci. Eng.* **1977**, *28*, 1-32.

[15] B. Zhao, B. Liu, R. Q. Png, K. Zhang, K. A. Lim, J. Luo, J. Shao, P. K. H. Ho, C. Chi, J. Wu, *Chem. Mater.* **2010**, *22*, 435-449.

[16] G. Zhang, C. B. Musgrave, *J. Phys. Chem. A* **2007**, *111*, 1554-1561.

[17] M. Stolte, S.-L. Suraru, P. Diemer, T. He, C. Burschka, U. Zschieschang, H. Klauk, F. Würthner, *Adv. Funct. Mater.* **2016**, *26*, 7415-7422.

[18] M. Sang, S. Cao, J. Yi, J. Huang, W.-Y. Lai, W. Huang, *RSC Adv.* **2016**, *6*, 6266-6275.

10.1002/chem.201900689

WILEY-VCH

Entry for the Table of Contents

FULL PAPER

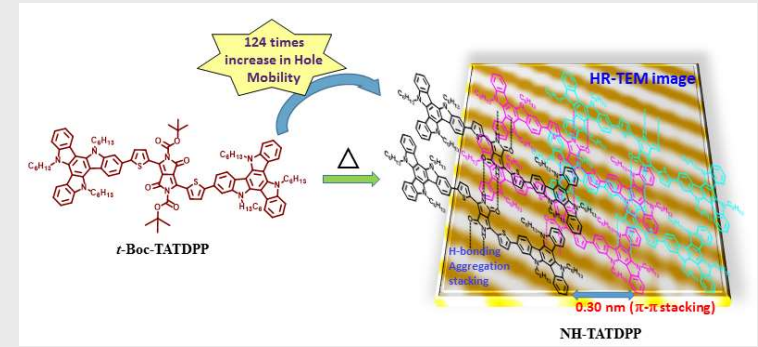

Soumyaditya Mula,[a][b][c] Tianyan Han,[d] Thomas Heiser,[d] Patrick Lévêque,[d] Nicolas Leclerc,*[a] A. P. Srivastava, [e] Amparo Ruiz-Carretero, [f] Gilles Ulrich*[a]*

Page No. – Page No.

Hydrogen-Bonding as Supramolecular tool for Robust OFET Devices

Hydrogen-bonded supramolecular network enhances the hole mobility in OFET by 2 orders of magnitude as compared to its parent compound.